Chapter 1

The minor bodies of the Solar System

The study of the minor bodies allows us to cast light on the origin and early evolution of the Solar System, since, according to the most generally accepted theory (Safronov 1979), they represent the "vestiges" of the left-over planetesimals from the early accretional phases of the proto-planetary disk. Even though minor bodies have been affected by thermal, dynamical, and collisional evolution, they contain a record of the initial conditions that existed in the solar nebula some 4.6 Gy ago. Thus, interpreting their present-day physical and orbital properties can tell us a lot about the compositional gradient of the nebula and the processes which governed the first phases of the Solar System at different heliocentric distances.

According to the most recent theories, commonly labeled as "Nice model" (Gomes et al. 2005; Morbidelli et al. 2005; Tsiganis et al. 2005), the current distribution of minor bodies is largely due to planetary migration occurred in the early history of the Solar System. Within this model, the four giant planets (Jupiter, Saturn, Uranus and Neptune) were originally found on near-circular orbits between ~ 5.5 and ~ 17 AU. Following the interactions with the planetesimals in a dense disk originally extended from the orbit of the outermost planet to some 35 AU, Saturn, Uranus and Neptune moved outwards, Jupiter moved slightly inward, while the outer primordial disk was almost entirely scattered, losing $\sim 99\%$ of its mass and producing the various populations of objects nowadays observable in the Solar System.

Moreover, during their history minor bodies have been subject to different transport mechanisms, as collisions, close approaches (mutual or with planets), and orbital resonances. The latter can lead to either long term stabilization of the orbits or be the cause of their destabilization, and are in general classified as secular resonances and mean motion resonances (e.g.,

Froeschle & Morbidelli 1994; Nesvorný & Morbidelli 1998). A mean motion orbital resonance occurs when two bodies (in this case, the minor body and a giant planet) have periods of revolution that are a simple integer ratio of each other (hereafter I adopt the convention that the p:q resonance denotes the resonance of p orbits of the inner object to q orbits of the outer object). A secular resonance occurs when the precession rate of the perihelion or ascending node of the minor body coincides with that of a giant planet.

Minor planets are divided into "groups" based on their current orbital and physical properties.

1.1 Dynamical classification

- **Trans-Neptunian Objects (TNOs):** after Pluto's discovery, the first object having an orbit that is completely trans-Neptunian was found in September 1992 (Jewitt et al. 1992; Jewitt & Luu 1993). Nowadays more than 1350 Trans-Neptunian Objects are known, and their investigation represents one of the most outstanding topics in contemporary planetary science, since these distant and icy bodies are considered to be the remnants of the planetesimals in the outer Solar System and to retain the most pristine (least altered) material that can presently be observed.

  From a dynamical point of view, they are in turn classified as (Gladman et al. 2008, see Fig. 1.1):

  Resonant objects: they lie in the about twenty identified mean motion resonances with Neptune, the most populated being the 3:2 resonance ($a = 39.4$ AU) which hosts Pluto among other bodies ("Plutinos").

  Scatter(ing/ed) Disk Objects (SDOs): Gladman et al. (2008) consider SDOs as those objects that are *currently* scattering actively off Neptune, without any assumption about their origin. With this nomenclature they exist down to $a = 30$ AU. At very large a (~ 2000 AU), where external influences become important, the inner Oort cloud begins.

  Detached objects: the term "detached", adopted from Delsanti & Jewitt (2006), indicates that these objects are essentially unaffected by the gravitational influence of Neptune, but not so far away that external influences are important to their current dynamics ($a \sim 2000$ AU).

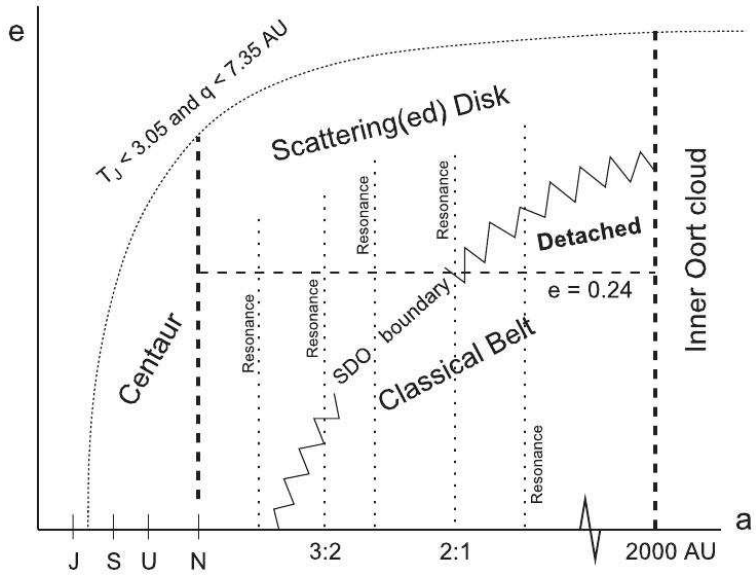

Figure 1.1 – Schematic illustration (not in scale) of the nomenclature for the outer minor bodies. From Gladman et al. (2008).

According to Gladman et al. (2008) they are nonscattering TNOs with large eccentricities ($e > 0.24$).

Classical objects: they are the remaining nonresonant, nonscattering, low-e TNOs. Gladman et al. (2008) divide this *classical belt* into an inner classical belt ($a < 39.4$ AU, nonresonant), an outer classical belt ($a > 48.4$ AU, nonresonant, and $e < 0.24$), and a main classical belt (or Cubewanos, after the first such object that was discovered, 1992 QB_1). Even if the current situation is not sufficiently clear to draw an arbitrary division, as stated by Gladman et al. (2008), many authors refer to two distinct populations in the classical belt based on orbital inclination (Levison & Stern 2001; Brown 2001): dynamically "hot" (high-inclination) objects, and dynamically "cold" (low-inclination) objects. In general, the latter present very red colors while the former have preferentially gray colors (Doressoundiram et al. 2002). On the basis of the fact that largest bodies in the hot population are bigger than those in the cold population, Levison & Stern (2001) suggested that the hot population formed closer to the Sun and was transported outward during the final stages of planet formation. Numerical simulations by Gomes (2003) showed that the hot population could find its origin in the migration of Neptune, which scattered the planetesimals originally

formed inside $\sim$ 30 AU. The current classical belt would hence be the superposition of these bodies with the local population, formed beyond 30 AU, which stayed dynamically cold. Assuming that the maximum size of the objects was a decreasing function of their initial heliocentric distance, this scenario explains why the biggest objects are all in the hot population. Moreover it explains the color difference between hot and cold objects, assuming that the color of bodies in the primordial disk varied with heliocentric distance (Morbidelli et al. 2008).

- **Centaurs:** according to the Minor Planet Center[1] (MPC) definition, a Centaur is an object with semimajor axis less than that of Neptune (30.1 AU) and perihelion distance larger than Jupiter's semimajor axis (5.2 AU). Gladman et al. (2008) classify them as having perihelion $q >$ 7.35 AU (halfway between the orbits of Jupiter and Saturn), semimajor axis less than that of Neptune, and Tisserand parameter[2] $\mathrm{T}_J > 3.05$. The intent of this definition is that the evolution of Centaurs is not currently controlled by Jupiter. Objects (60558) Echeclus and (52782) Okyrhoe, defined as Centaurs by the MPC, are accordingly reclassified as Jupiter coupled objects. The orbits of Centaurs are unstable, with lifetimes $\sim 10^6 - 10^7$ years, after which they can be ejected from the Solar System, impact the giant planets, or evolve into Jupiter Family Comets or Near Earth Objects (NEOs) (Horner et al. 2004). Centaurs are widely believed to come from the trans-Neptunian regions (Levison & Duncan 1997; Durda & Stern 2000) and to have been scattered into their present orbits by gravitational instabilities and collisions. Like Trans-Neptunian Objects, Centaurs accreted at low temperature and large solar distances, and must still contain relative pristine material. It has been suggested (e.g., Peixinho et al. 2003; Tegler et al. 2008) the presence of two distinct groups among Centaurs, one very red (Pholus-like) and one with neutral colors (Chiron-like). In this scenario very red Centaurs would have old surfaces, covered by an irradiation mantle, while blue objects might have younger surfaces rejuvenated by collisions and/or cometary-like activity.

- **Satellites of planets:** the *irregular* satellites of the outer planets,

[1] http://www.cfa.harvard.edu/iau/mpc.html

[2] The Tisserand parameter with Jupiter is defined as:

$$T_J = \frac{a_J}{a} + 2\sqrt{\frac{a}{a_J}(1-e^2)}\cos i \tag{1.1}$$

where a, e, i are the orbital semimajor axis, eccentricity, and inclination of the object and a_J is the semimajor axis of Jupiter.

generally orbiting on distant, inclined, eccentric, retrograde orbits, are believed to have been captured from heliocentric orbit during the early Solar System history (e.g., Nicholson et al. 2008). Conversely, *regular* satellites generally follow a close and prograde orbit, with low inclination and eccentricity, and are believed to have formed *in situ* (e.g., Magni et al. 1990). Neptune's satellite Triton represents an important exception, because despite of its close and circular orbit it is widely considered to be a captured body (e.g., Farinella et al. 1980; McKinnon 1991).

- **Trojans:** asteroids that are in a 1:1 mean motion resonance with a planet, around one of the two Lagrangian points of stability, L4 and L5, which lie 60° ahead of and behind the larger body. Until 1990 only Jupiter Trojans were known, with asteroids in the L4 group originally named Greeks, and those at the L5 point named Trojans. Nowadays, we refer to both groups as Trojans, and other than about 3700 Jupiter Trojans, four Mars Trojans and six Neptune Trojans are known.

- **Main Belt Asteroids (MBAs):** most of the $\sim$ 460000 known asteroids orbit the Sun between Mars and Jupiter, within the *main belt* (MB) which extends approximately from 2.06 AU (4:1 resonance with Jupiter) to 3.28 AU (2:1 resonance with Jupiter). In this region the last phases of the accretion of planetesimals into planets during the formative period of the Solar System were prevented by large gravitational perturbations by Jupiter. These perturbations caused too high relative velocities for the planetesimals to form planet-sized bodies. Moreover, strong Jupiter's gravity, through the mechanism of mean motion resonances (3:1, 5:2, 7:3), was responsible for the formation of the *Kirkwood gaps* in the distribution of main belt asteroids with semi-major axis (see Fig. 1.2). Wisdom (1983; 1987) looked for an analytical solution for the effect of resonances, and found chaotic orbits within the 3:1 and 2:1 Jovian mean motion resonances, and quasi-periodic orbits within the 3:2 resonance (where the so-called *Hilda* asteroids lie).

  The MB is widely believed to have suffered a strong collisional evolution, yielding a fragmentation of the original population in smaller and smaller bodies (Farinella et al. 1982). A major outcome of this process is the production of *dynamical families* among asteroids, with the parent body shattered or craterized to create a swarm of smaller asteroids sharing similar orbital elements (a, e, i). Current properties of families have been extensively studied to infer information on the physical processes that were responsible for their formation, and on the physical

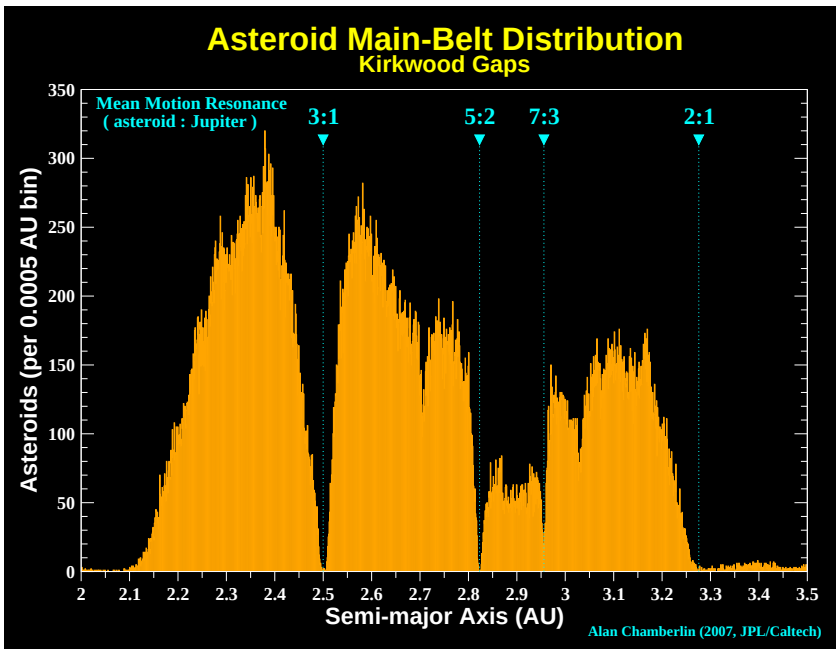

Figure 1.2 – Distribution of semimajor axis for asteroids. This graph was created in June 2007 using all asteroids with "well-determined" orbits (specifically, 156929 numbered asteroids).

properties of their parent bodies. From the current locations of the fragments in proper element space, interpreted in terms of differences in ejection velocities according to the classical Gauss equations, the kinematical properties of family-forming events can be derived (Cellino et al. 1999b). Moreover, spectroscopic investigations of family members can produce possible evidence of thermal differentiation of the original parent body (Cellino et al. 2002).

Recently (Hsieh et al. 2004; Hsieh & Jewitt 2006; Jewitt et al. 2009), the classical distinction between (inert, rocky) asteroids and (active, icy) comets has been complicated significantly with the discovery of the class of Main Belt Comets (MBCs). There are currently four known MBCs (Fig. 1.3), which orbit completely within the main asteroid belt: 133P/Elst-Pizarro, P/2005 U1 (Read), 176P/LINEAR (1999 RE_{70}), and P/2008 R1 (Garradd). Unlike all other comets, which originated in the outer Solar System, MBCs appear to have formed where we see them today. Hence, it is supposed that they have been dormant until very recently (otherwise they would have exhausted their ice supplies long ago), and that their activity has been triggered by impacts excavating buried volatiles. The discovery of MBCs demonstrates that

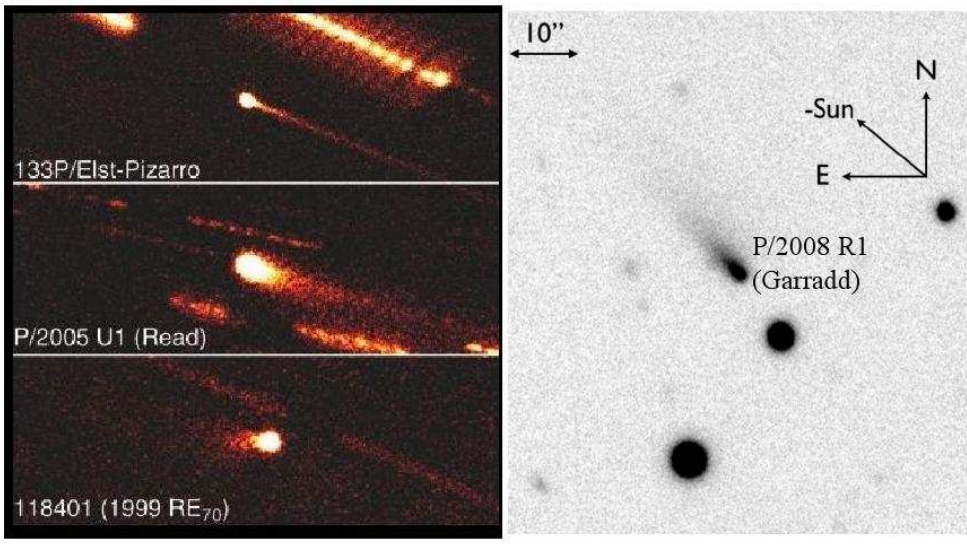

Figure 1.3 – Pictures of the four known MBCs (Hsieh & Jewitt 2006; Jewitt et al. 2009).

ice exists and may be quite common in the MB, and supports the theory that outer main belt could be a likely source of terrestrial water (Morbidelli et al. 2000; Albarède 2009).

- **Near Earth Objects (NEOs):** Near Earth Objects are asteroids (NEAs) and comets (NECs) with perihelion less than 1.3 AU. At the present time more than 6500 NEOs are known, less than 100 being comets (probably coming mostly from Jupiter Family Comets, as suggested by DeMeo & Binzel 2008). Their lifetimes are $\sim 10^6 - 10^8$ years, after which either they impact the Sun or a planet, or are ejected from the Solar System. The NEO population is replenished from particular zones in the main belt, which provide NEOs via powerful and diffusive resonances (Morbidelli et al. 2002).

1.2 Physical characterization and observing techniques

The differences presented by minor bodies at varying distances from the Sun are directly due to the compositional gradient of the primordial nebula with heliocentric distance. In the inner protoplanetary disk, heated by the

Sun, ices and gases could not condense, leaving mainly rocky and metallic minerals. Conversely, in the cold outer disk, ices and gases, as well as silicates and metallic compounds, could condense.

The understanding of the physical (as well as dynamical) properties of the minor body populations can therefore provide crucial information to investigate the structure and the early evolution of the Solar System at different distances from the Sun.

Different observing techniques can be adopted to characterize the physical nature of minor bodies. Among them the most widely used are *photometry* and *reflectance spectroscopy*.

1.2.1 Photometry

Colors: The investigation of photometric colors represents the best technique to study a large number of (eventually faint) objects (e.g., TNOs, see section 4.2). Even if photometric colors cannot provide firm constraints on the surface composition, since they depend also on scattering effects in particulate regoliths and viewing geometry, they nevertheless bring important information and they can be used to classify the observed objects in different groups that reasonably indicate different composition and/or evolutional history. For example, on the basis of photometric colors, taxonomies were firstly created for asteroids a few decades ago, and recently also for Centaurs and TNOs (see sections 1.3.1 and 1.4.1).

Phase curves: Bowell et al. (1989) have found a relationship (*phase curve*) between the observed magnitude of asteroids and the phase angle α, which can be written as:

$$H(\alpha) = H - 2.5log[(1-G)\varphi_1(\alpha) + G\varphi_2(\alpha)] \tag{1.2}$$

where

- $H(\alpha)$ is the asteroid's V magnitude reduced to unit heliocentric (r) and geocentric (Δ) distances, $H(\alpha) = V - 5log(r\Delta)$, function of the phase angle of observation;
- H is the *absolute magnitude*, i.e. at $\alpha = 0°$;
- G is the angular coefficient of the phase curve, the so-called *slope parameter*;

- $\varphi_1(\alpha)$ and $\varphi_2(\alpha)$ are two functions of α defined as:

$$\varphi_1(\alpha) = exp\Big[-3.33\Big(tan\frac{\alpha}{2}\Big)^{0.63}\Big] \tag{1.3}$$

$$\varphi_2(\alpha) = exp\Big[-1.87\Big(tan\frac{\alpha}{2}\Big)^{1.22}\Big] \tag{1.4}$$

Absolute magnitude H and slope parameter G represent two very important photometric parameters, which can be determined by:

$$H = -2.5log(a_1 + a_2) \tag{1.5}$$

$$G = \frac{a_1}{(a_1 + a_2)} \tag{1.6}$$

where a_1 and a_2 are two auxiliary variables, constant for each asteroid, which can be set with a least squares fit of $H(\alpha)$ and α to the relation:

$$H(\alpha) = -2.5\log[a_1\varphi_1(\alpha) + a_2\varphi_2(\alpha)] \tag{1.7}$$

Slope parameter G relates to the surface's albedo (Tedesco 1989; more recently, Carvano 2008), which is in turn related to the so-called *opposition effect*, a surge in brightness observed when the object is near opposition. The amplitude and width of opposition effect depend on surface albedo in a non-monotonic way with maximum for the moderate albedo bodies which is impossible to explain neither by coherent-backscatter effect (a preferential tendency for light scattered along conjugate paths in the regolith to constructively interfere at small phase angles) nor shadow-hiding effect (regolith particles progressively occult their own shadows as the phase angle decreases to zero) alone. Attempts to derive a physically motivated photometric model that incorporates both these effects, so far have not yielded a widely accepted model (Belskaya & Shevchenko 1999; Shkuratov & Helfenstein 2001).

From the absolute magnitude, once also the geometric (visual) albedo p_v is known, an estimation of the object's diameter D is possible, through the relation (Tedesco et al. 1992):

$$D = \frac{1329 \times 10^{-H/5}}{\sqrt{p_v}} \tag{1.8}$$

Light curves: A very powerful tool for retrieving information about the minor bodies is the analysis of their photometric light curves, which are

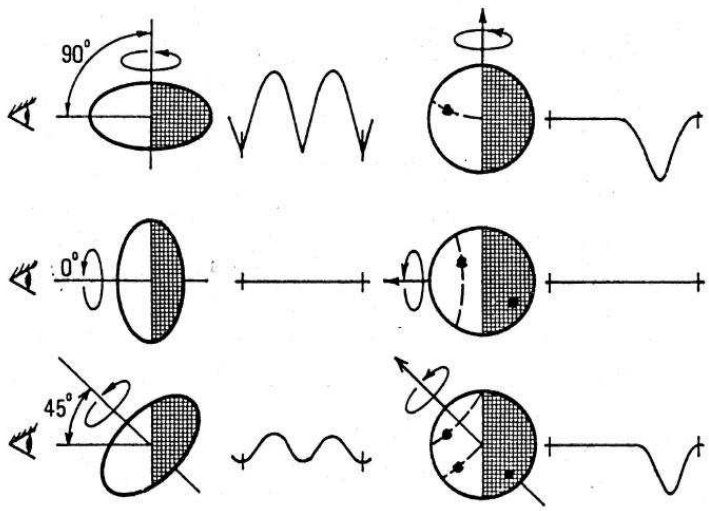

Figure 1.4 – Examples of body profiles with corresponding light curves.

functions of the rotational period, spin axis orientation, shape, and large-scale surface structure of the observed objects (Fig. 1.4).

To retrieve the rotational periods of the investigated bodies, in this work I followed the method developed by Harris et al. (1989a), performing a Fourier analysis of the *composite* (i.e. combining data from different observing nights) light curves. These latter are described as:

$$V(\alpha, t) = \overline{V}(\alpha) + \sum_{k=1}^{n} \left[A_k \sin \frac{2\pi k}{P}(t - t_0) + B_k \cos \frac{2\pi k}{P}(t - t_0) \right] \qquad (1.9)$$

where

- $V(\alpha, t)$ is the computed reduced magnitude at phase angle α and time t;
- $\overline{V}(\alpha)$ is the mean magnitude at phase angle α;
- A_k and B_k are Fourier coefficients;
- P is the rotational period;
- t_0 is a zero-point time, chosen near the middle of the time span of the observations.

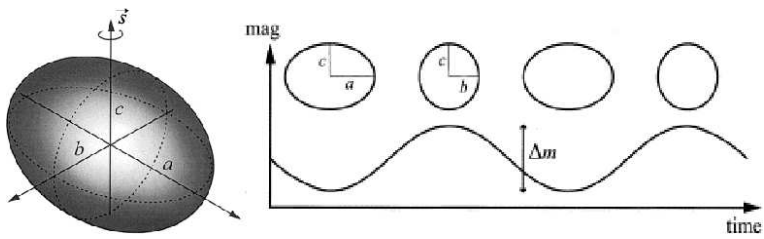

Figure 1.5 – Light curve produced by a triaxial ellipsoid.

A least squares fit of the data to the function 1.9 is performed to find the rotational period which minimizes the errors. Of course, the above procedure works only for short-arc solutions, spanning only a few days. Differently, errors due to uncertainty of the period and changing structure of the light curve (because of different viewing geometry of the observations) could be significant.

Assuming that the observed light curve amplitudes are due only to the bodies' shapes, with negligible albedo variations on their surfaces, a lower limit to the axis ratio a/b comes from the relation:

$$\Delta V = 2.5 \log \left(\frac{a}{b} \right) \tag{1.10}$$

where ΔV is the maximum light curve amplitude (reached in equatorial view, i.e., at an aspect angle $\xi = 90°$) produced by a triaxial ellipsoid with axes $a > b > c$ rotating about the c axis (Fig. 1.5; e.g., Binzel et al. 1989).

1.2.2 Reflectance spectroscopy

Visible and near-infrared (NIR) spectroscopy constitutes the most sensitive and broadly applied technique for characterizing the surfaces of the minor bodies. At these wavelengths thermal emission from the surface is negligible (except low-albedo NEOs which are warm enough to emit detectable thermal flux at 2.5 μm, see Rivkin et al. 2005), while reflected sunlight presents absorption features due to the interaction between incident photons and the surface materials, via electronic and vibrational transitions which are diagnostic of specific mineral or molecular species. The spectral parameters (e.g., band position, depth, shape) of these absorption features are related to the specific composition of the individual material. Nevertheless, the interpretation of the observed reflectance spectra is far from being unambiguous, since spectral features of the different materials combine in a nonlinear way. Hence the most straightforward way to indentify materials on minor bodies'

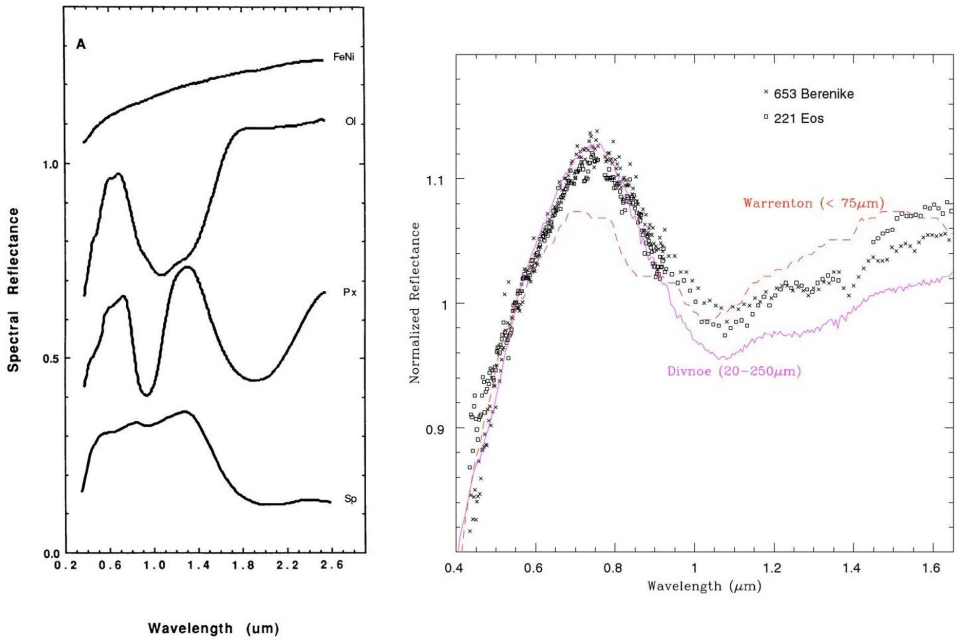

Figure 1.6 – *(left)* Reflectance spectra of several minerals which are important for asteroid spectra interpretation: olivine (Ol), pyroxene (Px), iron-nichel metal (FeNi), spinel (Sp). From Gaffey et al. (1993). *(right)* Reflectance spectra of (221) Eos (squares) and (653) Berenike (crosses) versus spectra of the CO3 chondrite Warrenton and the anomalous stone Divnoe. In parenthesis it is indicated the grain size of the sample. From Mothé-Diniz & Carvano (2005).

surfaces is by comparison with laboratory spectra of meteorites, minerals and ices (Fig. 1.6). In particular, rather than the overall spectrum, it is important to well fit those spectral parameters that are diagnostic of the presence and composition of particular mineral species. For example, the wavelength positions of the 1 and 2 μm features in pyroxene spectra are a function of the Ca and Fe contents of the individual mineral samples, while the ratio of 2 μm band area to 1 μm band area in olivine-orthopyroxene mixtures is directly related to the ratio of pyroxene to olivine abundances (e.g., Gaffey et al. 2002).

Starting from this, a more detailed picture of the surface compositions can be obtained with *spectral modeling*, i.e. calculating synthetic spectra based on radiative transfer formulations and laboratory measurements of optical constants (Fig. 1.7).

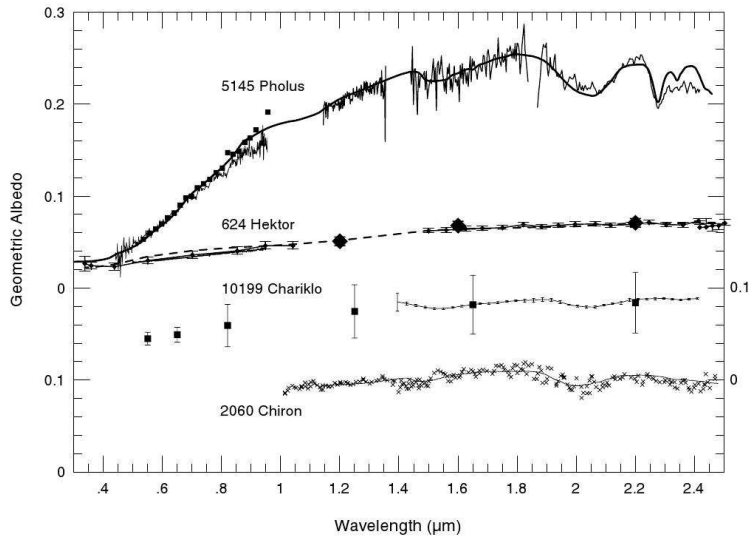

Figure 1.7 – Reflectance spectra of three Centaurs and Jupiter Trojan (624) Hektor, with superimposed models. For example, the model for (2060) Chiron consists of H_2O ice and olivine. All three Centaurs show the prominent 2 μm H_2O ice band, with also indications of the weaker 1.5 μm band. There is no spectral evidence for ice on Hektor. For Chiron the scaling to geometric albedo is approximate, the ordinate for the spectrum of (10199) Chariklo is given on the right side of the figure, while the ordinate for both Hektor and (5145) Pholus is given on the left side of the figure. From Barucci et al. (2002) and references therein.

The optical constants of a material are the real and imaginary components of the complex refractive index, $\tilde{n} = n + ik$, which describes the interaction of electromagnetic radiation with that material. In this representation, n is the "real" index of refraction, and k is the extinction coefficient, which describes the damping of an electromagnetic wave in the material. Both n and k are wavelength dependent. As electromagnetic radiation passes through the material, some fraction is absorbed per unit distance it travels, according to the Beer-Lambert law, which allows the calculation of the absorption coefficient α. If λ is the (vacuum) wavelength of the electromagnetic radiation of interest, then the imaginary index is $k = \lambda\alpha/4\pi$.

For atmosphereless bodies, the two major points of the theory of radiative transfer are solving the integral equation and developing a statistical representation of the regolith individual particles to relate particle properties to scatterer properties. The integral equation and statistical approaches are generally combined to perform spectral modelings of particulate regolith

surfaces. The local mean properties of scattering and absorption are determined by the statistical method, while the integral equation method gives the bidirectional reflectance of a medium composed of such particles. Such a combined technique allows the measured brightness to be related to the microscopic quantities.

The two major theories which are used to model minor bodies' surfaces have been developed by Hapke (1981, 1993) and Shkuratov et al. (1999). Through them it is possible to determine the reflectance spectra or the albedo of a medium from individual physical properties of the different chemical components (with known optical constants). The main differences between the approaches of Shkuratov and Hapke are the treatment of the phase function (which is calculated rather than assigned as an explicit parameter, respectively) and the number of free input parameters (relative amounts, grain size and optical constants of the selected components in Shkuratov, much more in Hapke). Both formulations allow mixing of materials in a variety of ways that include molecular as well as intimate mixtures. Molecular mixtures consist of inclusions in a medium of contaminant particles. Intimate mixtures are the so-called "salt and pepper" mixtures.

A comparison between Hapke and Shkuratov models can be found in Poulet et al. (2002).

1.2.2.1 Aqueous alteration

"Aqueous alteration" is a chemical alteration of a material by the interaction of that material with liquid water. Its action has been inferred for many asteroids, especially in the middle main belt, based on reflectance spectroscopy which shows absorption features (mainly in the 0.4-0.9 and 2.4-3.6 μm regions) diagnostic of or associated with hydrated minerals (for a review, see Rivkin et al. 2002).

Aqueous alteration in asteroids is supposed to be connected to some early heating event either due to the decay of ^{26}Al, a now extinct short-lived isotope, or to electrical induction heating due to a strong early (T-Tauri phase) solar wind (Jones et al. 1990), and hydrated silicates (*phyllosilicates*) can be used as very sensitive tracers of thermal history (Hiroi et al. 1996). In addition to altering olivine and pyroxene to form hydrated silicates (e.g. serpentine), the aqueous alteration process produces oxidized Fe that has absorption bands in the visible and UV spectral regions. Moderate subsequent heating can alter the depth or eliminate some or all of these bands. Hence the study of hydrated minerals on asteroids, and of their distribution with heliocentric distance, provides insight on important issues as the homogeneity of the solar nebula, the heat sources present, and how much mixing

of planetesimals occurred.

Studies of dark, volatile-rich asteroids with orbits beyond 3.5 AU have shown that only a few of them contain in their spectra features typical of aqueous alteration (Rivkin et al. 2002). The prevalent explanation is that induction heating is much less efficient further away from the Sun (e.g., Jones et al. 1990). If this interpretation is correct, aqueous alteration would not be expected for TNOs. One should note, however, that Cruikshank et al. (2001) have suggested that the lack of hydration features in asteroid spectra at large distances from the Sun might be due instead to an increasing amount of spectrally opaque material on their surfaces.

Actually, some features detected in the visible spectra of some TNOs have been interpreted in terms of the presence of aqueously altered minerals on their surfaces (de Bergh et al. 2004; Fornasier et al. 2009). How aqueous alteration processes could have occurred in the outer solar System is not well understood, and it is also possible that some hydrated minerals formed directly in the solar nebula. Large TNOs may have been subjected to significant radiogenic heating (Luu & Jewitt 2002), but it remains to be seen if this would have been sufficient for aqueous alteration of the anhydrous material inside the TNOs, and also a mechanism capable of transporting enough heat to the surface would be required. Another way to heat a TNO is by impacts, which could have provided a transient heat source. However, the heat generated and the duration of the heating episode(s) may not have been sufficient for aqueous alteration of minerals (e.g., Kerridge & Bunch 1979).

1.2.2.2 Space weathering

Solar radiation, cosmic rays, and micro-impacts are inferred to alter the surface of atmosphereless bodies and progressively to change their reflectance spectra. "Space weathering" was first studied for the Moon, since lunar soils returned from Apollo missions have optical properties that differ significantly from those of pristine lunar rocks (Conel & Nash 1970). After that, time-related space weathering processes have often been invoked to interpret spectra of Solar System atmosphereless bodies.

In the laboratory it is possible to reproduce space weathering processes on relevant materials (analogues), such as silicates, ices, and carbons, and in a few cases on materials directly coming from space, i.e. meteorites, interplanetary dust particles (IDPs), and grains collected on Earth or from sample return missions. Solar wind and cosmic ion irradiation can be correctly simulated by keV-MeV ion irradiation, while micro-meteorite bombardment can be simulated by impact experiments (Brunetto 2009).

The effects of space weathering are different according to the heliocentric

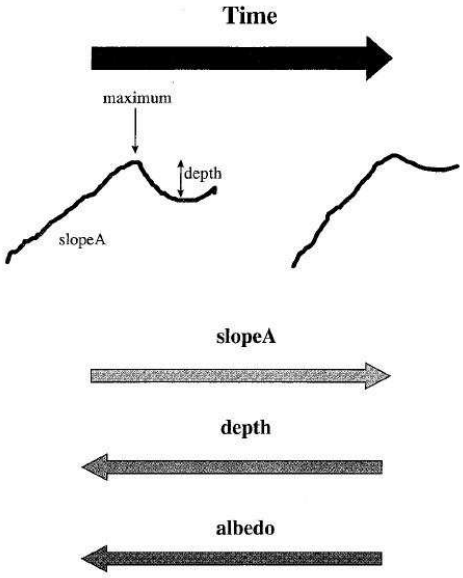

Figure 1.8 – Behavior of space weathering and spectral parameters. From Doressoundiram et al. (1998).

distances of the bodies and their surface composition. In the inner Solar System, silicate surfaces grow darker in time, while their reflectance becomes redder than the spectra of their constituting rocks (Fig. 1.8), as suggested by many authors (e.g., Doressoundiram et al. 1998; Chapman 2004), and confirmed by recent laboratory experiments on ordinary chondrites and silicates, irradiated with heavy ions at keV energies (Strazzulla et al. 2005; Brunetto & Strazzulla 2005).

As an example of how the knowledge of the mechanisms which determine surface evolution can help the interpretation of asteroids' observations, Binzel et al. (2004) invoked space weathering processes to explain the trend of the spectral slopes of NEOs as a function of size. These authors noticed that the visible spectral slope of NEOs have a high dispersion for the smallest objects, and are less dispersed for larger sizes. A possible cause of that could be the effect of space weathering processes: since smaller NEOs have shorter collisional lifetimes than larger ones, they could have younger (less reddened) surfaces, which explains why the dispersion of spectral slopes among them can be expected to be higher than among larger NEOs.

In the outer Solar System cosmic rays should lead to the selective loss of hydrogen in surface materials, and promote the formation of chemically complex polymers, many of which are dark in colour and spectrally red, due to their high carbon abundance (e.g., Andronico et al. 1987). Natural bitu-

mens (e.g. asphaltite, kerite) appear to be reasonably good reference analogs for refractory extraterrestrial organic matter, in terms of spectral properties and chemical structure, especially for TNOs and comets. Their visible and near-infrared spectra flatten after ion irradiation (Moroz et al. 2004). The same weathering process on originally low absorbing ices induces color variations that can reproduce the observed spectral variety of outer Solar System objects (Brunetto et al. 2006). The obtained organic refractories are generally characterized by low albedo and red spectral slope. Thus, the space weathering color trend is not yet well established, due to a strong dependence on the unknown original composition.

1.3 Inner Solar System: up to Jupiter

In the Inner Solar System we find asteroids belonging to different populations: NEAs, MBAs, Jupiter Trojans. As already said, their surfaces mainly present rocky and metallic non-volatile minerals.

1.3.1 Taxonomy

From the seventies of last century, many authors tried to define taxonomic schemes based on observational properties (spectrum, colors, albedo, etc.) of the asteroids. The common intent of these taxonomies is to group asteroids in different classes which are thought to correspond to similar surface composition and/or thermal evolution. It is worth noting that, while the membership to different classes is probably a sign of a substantial difference in the composition, the opposite is not necessarily true, as two bodies belonging to the same taxon may not have the same mineralogical composition. Nevertheless groups' members are supposed to be composed by a limited number of "assemblages".

A very robust taxonomy is that proposed by Tholen (1984, 1989) based on broad band spectrophotometric colors obtained during the Eight-Color Asteroid Survey (ECAS, Zellner et al. 1985), which observed 589 asteroids in the wavelength range 0.3 - 1.1 μm. Tholen identified 14 classes, each denoted by a single letter. In addition to the two "classical", already recognized classes (Chapman et al. 1975), the C (carbonaceous) and S (silicaceous) types, Tholen identified six other spectrally distinct groups of objects, labeling them A, B, D, F, G, and T. Three further classes, labeled as E, M, and P, had featureless ECAS spectra and could only be separated based on their albedos (Barucci et al. 1987 were the first to consider the albedo as a parameter for the classification, in addition to ECAS colors, adding more physical

interpretation to their taxonomic scheme). A generic X-class designation was assigned whenever albedo information was not available for objects belonging to these spectral classes (Tholen 1989). Three asteroids did not fall into any of the above classes and were assigned unique designations: Apollo (Q-type), Dembowska (R-type), and Vesta (V-type). When the classification was uncertain, multiple letter designations were assigned.

A most recent classification is the taxonomy based on the second phase of the Small Main-Belt Asteroid Spectroscopic Survey (SMASSII, Bus & Binzel 2002b,a), which defines 26 different classes attempting to keep to the Tholen taxonomy as much as possible. Three major groupings (the S-, C-, and X-complexes) are introduced, as well as a new L-class. Asteroids with intermediate spectral characteristics are assigned multiletter designations. In 2009, the Bus & Binzel taxonomy has been extended to consider also near-infrared data by DeMeo et al. (2009a).

As discussed above, the taxonomic classification is not directly based on composition or mineralogy. Nevertheless, the members of the same taxon have similar spectra and hence would present a limited suite of constituents. Table 1.1 reports the inferred associations of each Tholen taxonomic class with different mineral assemblages.

Gradie et al. (1989) showed that the distribution of the asteroid taxonomic classes is a function of heliocentric distance. For example, the silicaceous, volatile-poor S-types dominate the inner main belt; low-albedo, carbonaceous C-types are concentrated in the middle/outer main belt; dark, ultra-carbonaceous, volatile-rich D-types are more abundant at larger distances from the Sun (Fig. 1.9). This suggests that a compositional gradient was present in the solar nebula, and that asteroid surfaces have undergone different degrees of thermal processing, in function of their heliocentric distance.

This guess is strengthened by the many associations that have been established (on the basis of their spectra and albedos) between different asteroid taxonomic classes and petrologic types of meteorites.

1.3.2 Relationships among asteroids and meteorites

Meteorites belonging to the same compositional group are believed to come from the same parent body or several similar parent bodies, and meteorite analogues have been assessed for different asteroid taxonomic classes (Table 1.1). Different thermal histories are supposed to have produced the different petrologic types (Fig. 1.10): ordinary chondrites (similar to Q-type asteroids) have undergone modest thermal evolution over the age of the So-

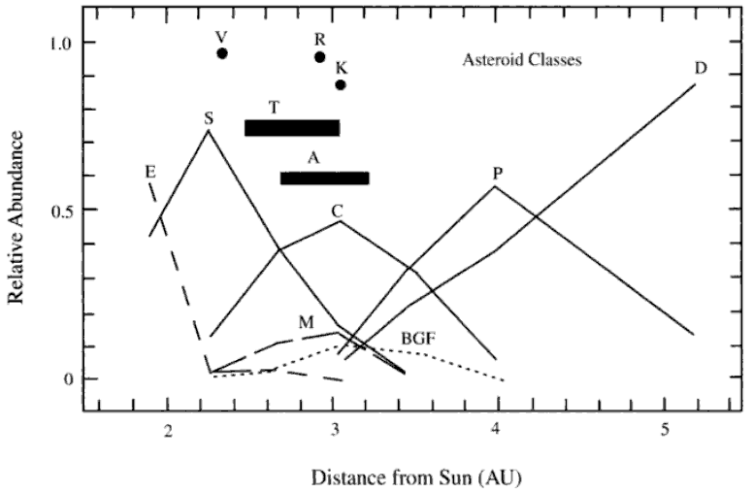

Figure 1.9 – The distribution of classes in the asteroid belt. From Bell et al. (1989).

lar System, while carbonaceous chondrites (similar to C-type asteroids) are inferred to be more primitive. In some cases a strong relation has been found between a group of meteorites and a specific object candidate to be the parent body. For example, from dynamical and spectroscopic constraints, it has been suggested that (6) Hebe may be a significant source of the ordinary chondrites (Migliorini et al. 1997; Gaffey & Gilbert 1998).

Nevertheless, the link between asteroids and meteorite types is not completely understood. It has been noticed that there is a significantly greater apparent mineralogical diversity among asteroids than among meteorites (Gaffey 1999), hence meteorites would be an incomplete sample of the mineralogy present among asteroids. Also the study of the cosmic ray exposure ages of meteorites indicates the presence of discrete groups at different ages (Perron & Zanda 2005). This seems to suggest that the delivery of meteorites is not a continuous flux: it should be due to a few events and would be drawn by some selection effects, e.g. the proximity of the parent body to a chaotic zone in the asteroid main belt and/or the structure and nature of the parent body itself.

A problem known as the "S-type conundrum" has persisted for nearly two decades, but nowadays appears to have found a solution. Stated very simply, the conundrum is that 80% of all meteorites that fall to Earth are ordinary chondrites, whose spectral analogues (Q-type objects) are instead quite rare among the asteroids. Binzel et al. (1996) suggested a possible solution of this conundrum. They showed that NEOs have spectral features which span

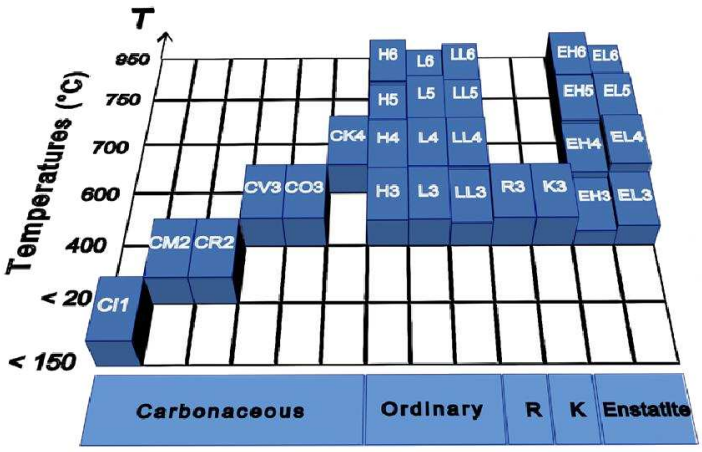

Figure 1.10 – Chondrite meteorites classification as a function of the estimated temperature required for producing the petrologic types. R and K on the bottom indicate Rumuruti and Kakangari, respectively. The level of each box in the third dimension gives the relative proportions of the various types for each chondrite group.

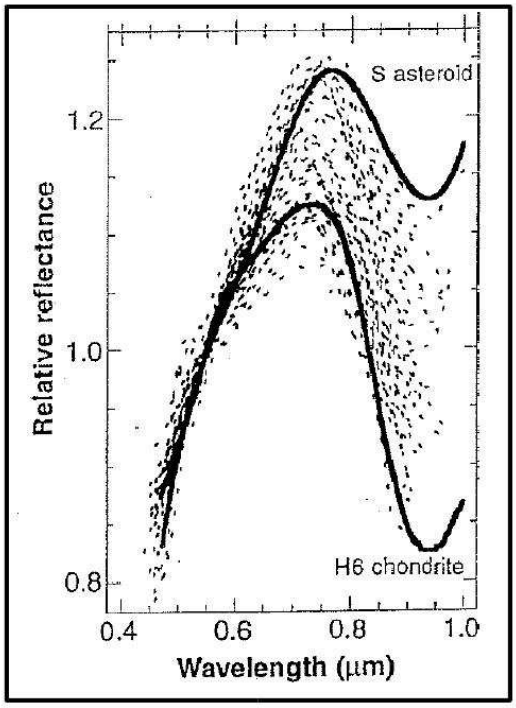

Figure 1.11 – Reflectance spectra of NEOs fill the interval between those of main belt S-types and ordinary chondrites. From Binzel et al. (1996).

Table 1.1 – Mineral assemblages and meteorite analogues inferred for each asteroid taxonomic type.

Tax. type	Minerals	Possible meteorite analogues
A	Olivine, Fe-Ni	Olivine achondrites, pallasites, olivine-metal partial melt residues
V	Pyroxene, feldspar	Basaltic achondrites (eucrites, howardites, diogenites)
R	Olivine, orthopyroxene	Olivine-pyroxene cumulates, olivine-pyroxene partial melt residues
E	Enstatite (Fe-free pyroxene)	Enstatite achondrites (aubrites), Fe-bearing enstatites, Fe-bearing aubrites
M	Fe-Ni, enstatite	Iron meteorites, enstatite chondrites
S	Fe-Ni, olivine, pyroxene	Pallasites, olivine-dominated stony-iron, ordinary chondrites
Q	Olivine, pyroxene, Fe-Ni	Ordinary chondrites
C, B, G, F	Fe-bearing hydrated silicates, C	Carbonaceous chondrites
P	Anhydrous silicates, organics	none
D	Organics, anhydrous silicates	none
T	?	?

the range between the domains of ordinary chondrite meteorites and the most common S-type MBAs (Fig 1.11). They concluded that this range could arise through a diversity of mineralogies and regolith particle sizes, as well as through a time-dependent surface alteration mechanism (space weathering, see section 1.2.2.2). In this last case, asteroids most closely resembling ordinary chondrite meteorites would be those with the youngest surfaces.

1.3.3 Asteroids seen by space missions

To date several asteroids have been investigated by space missions. *In situ* study of asteroids provided critical information unavailable from ground-based observations, and gave us a big improvement to our knowledge about the nature of these bodies.

Visited objects have been studied in detail, obtaining data about their size, shape, rotation, and surface properties. Fly-bys can also give us the asteroid mass, with a subsequent determination of the mean density after a reliable estimate of volume. All of this information can lead to important hints about the physics of the investigated body, and the comparison with ground-based observations can provide the *ground truth* for studies of the asteroids which will be never visited by a space mission.

On October 1991 the Galileo spacecraft, during its travel towards Jupiter, carried out the first ever fly-by of an asteroid, (951) Gaspra (Fig. 1.12, left).

Figure 1.12 – *(letf)* Asteroid (951) Gaspra in a mosaic of two images taken by the Galileo spacecraft from a range of 5300 km, some 10 minutes before closest approach on October 29, 1991. *(right)* Asteroid (243) Ida and its moon Dactyl, the first discovered orbiting an asteroid. From http://solarsystem.nasa.gov.

Gaspra resulted to be a higly irregular, cratered body with principal diameters of 18.2 x 10.5 x 8.9 km. Flat surfaces, ridges, and prominent grooves suggested that this asteroid has a monolithic structure (Stooke 1996). Albedo and color variations observed in correlation with morphological features suggested that Gaspra is covered with a thin regolith which has migrated downslope in some areas (Belton et al. 1992). The low rate and size distribution of impact craters allowed an estimation of the surface age of only 200 million years, possibly suggesting a recent break-up event for the birth of this asteroid (Chapman et al. 1996).

On August 1993, Galileo encountered a second MBA, (243) Ida (with dimensions of 56 x 24 x 21 km). Especially noteworthy was the discovery of a small ($\sim$ 1 km) natural satellite, Dactyl, in orbit around Ida at a distance of $\sim$ 100 km (Fig. 1.12, right). This represented the first observation of a binary system among asteroids. Ida presents a high craterized surface, with an estimated upper limit for the age of $\sim$ 1 Gyr (Belton et al. 1996), while the age of Dactyl should be in the 100-200 Myr range. Moreover, Dactyl's collisional disruption lifetime is very short compared with Ida's age, hence it must be a re-accumulated satellite from previous ejecta (Davis et al. 1996).

Both Gaspra and Ida are S-type asteroids.

On June 1997, the NEAR (Near Earth Asteroid Rendezvous, later renamed Shoemaker) spacecraft flew-by the more primitive C-type MBA (253) Mathilde. Its mass was well determined, with a resulting value of 1.033 $\pm$

0.044×10^{20} g (Yeomans et al. 1997). Coupled with a volume estimate from the imaging data, this value yielded a bulk density for Mathilde of only 1.3 g/cm^3, probably indicating a "rubble pile" structure for this asteroid. Nevertheless structures as a 20-km long scarp (on a body of diameter $\sim$ 53 km) and polygonal craters indicate that Mathilde is not completely strengthless (Cheng 2004).

On February 2000, NEAR Shoemaker was placed in orbit around (433) Eros, the main target of the mission. For the first time ever a "rendezvous" mission with a minor body was performed. Eros is a S-type NEA with an elongated shape (33 x 13 x 13 km). Collected images showed a high quantity of boulders and big craters, but only a few of small craters. A possible explanation is that the small size and low gravity of Eros may result in redistribution or loss of ejecta due to seismic shaking, thus preferentially destroying small craters formed in such regolith (Chapman et al. 2002). On 12 February 2001 the mission was ended with a controlled descent on Eros. Data with the X-ray/Gamma-Ray Spectrometer (XGRS) were collected, to study the surface composition. It resulted that low aluminum abundances for all regions argue against global differentiation of Eros. From element abundances it has been derived a relatively primitive, chondritic composition, with possible signatures of limited partial melting or impact volatilization (Trombka et al. 2000).

Hayabusa (formerly known as MUSES-C), the first sample return mission from an asteroid, reached on September 2005 its target, the NEA (25143) Itokawa (Fig 1.13). After a complete topographic and spectroscopic analysis of the surface, in November 2005 it landed on the asteroid and attempted to collect samples. Because of some technical problems, it is not sure if the collection of material in the storage capsule succeeded. The spacecraft is scheduled to return to Earth by June 2010. Nevertheless, in situ analysis already brought many results. Itokawa appears to be a contact binary *rubble pile* asteroid, with a lack of impact craters. Its surface is divided in two parts: the first, rough and characterized by boulders; the second, smooth and covered by regolith. A minimum in the gravitational potential has been observed in correspondence of the limit between these two parts. It has been suggested a correlation between this minimum and the high quantity of regolith present in this region, caused either by seismic movements due to impacts or by gravitational effects induced by the close passages to the Earth (Fujiwara et al. 2006, and references therein). Some color difference is present over the surface but no mineralogical differences have been found (Ishiguro et al. 2007).

Two further missions planned to visit asteroids are currently flying: Dawn,

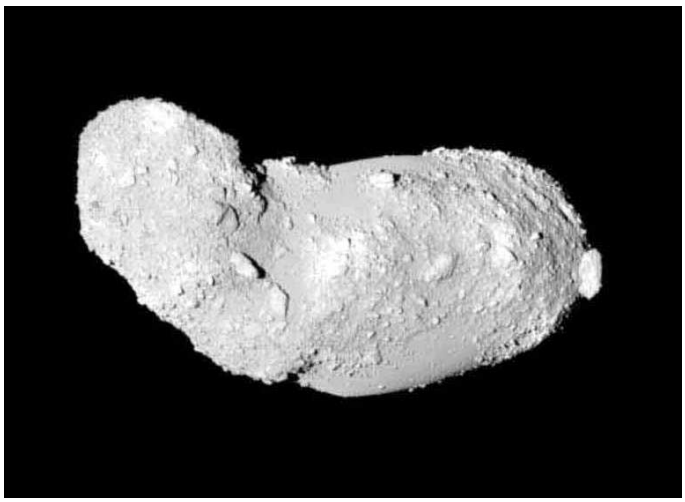

Figure 1.13 – Asteroid (25143) Itokawa taken by the Hayabusa probe.

which will orbit Vesta (arrival in 2011) and Ceres (arrival in 2015), the two largest bodies in the main belt; and Rosetta (see chapter 3), which flew-by asteroid (2867) Steins in September 2008 and will fly-by (21) Lutetia in July 2010, on its way to comet 67P/Churyumov-Gerasimenko.

1.4 Outer Solar System: far from the Sun

In the outer regions of the Solar System, far from the Sun, formation temperatures were sufficiently cold to let ices to condense and remain stable, allowing the Centaurs and TNOs nowadays observable to be a mixture of rocks and ices.

1.4.1 Taxonomy

A taxonomic scheme based on color indices has recently been developed for TNOs and Centaurs by Barucci et al. (2005a), using G-mode analysis (Coradini et al. 1977, see appendix A).

As already did in the past for the asteroids (see section 1.3.1), the investigation of broadband colors of the far (faint) minor bodies in the outer Solar System provides a first hint on their possible different composition and/or evolutionay history. Such an approach to studying the physical properties of asteroids has resulted in a taxonomy scheme based mostly on surface colors and albedos, and has become an efficient tool in asteroid science.

A two-letter designation for the identified groups is introduced to distinguish TNO taxonomy from asteroid taxonomy (Fig. 1.14):

The RR ("red") group contains the reddest objects of the Solar System. This behavior could be explained by the presence of large amounts of tholins on the surface (tholins are complex organics produced by the irradiation of mixtures of cosmically abundant reducing gases and ices, Roush & Cruikshank 2004), as it results from composition models available for some of them (Barucci et al. 2005a, and references therein).

Objects having neutral colors with respect to the Sun are classified as the BB ("blue") group. Typically their spectra are flat and slightly bluish in the near-infrared. The H_2O absorption bands seem generally stronger than in the other groups (Barucci et al. 2005a, and references therein).

The IR group includes moderately red objects, while the BR group is an intermediate group between BB and IR, with its colors closer to those of the IR group.

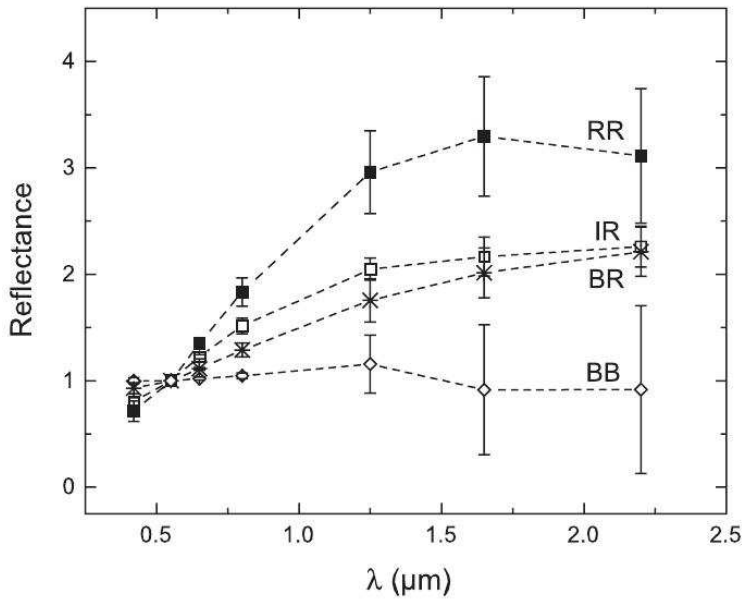

Figure 1.14 – Average reflectance values for each TNO taxon, normalized to the Sun and to the V colors. From Fulchignoni et al. (2008).

1.4.2 Surface composition

Even if only the brightest TNOs have been spectroscopically investigated, because of the faintness of these bodies, interesting results have been obtained regarding their surface composition.

A remarkable variety appears, with the presence of several ices on objects belonging to all of the four taxonomic classes discussed in the previous section. Barucci et al. (2006), using available literature, searched for correlations between the taxonomic group and the presence of ice, but none were found. Nevertheless the authors suggested that non-icy bodies seem to be concentrated in the RR group, as the probable presence of organic compounds (see previous section) on these bodies could hide the present ices. Moreover, it seems that ices are generally more abundant on BB-types than in the other taxa.

A relationship between the size of the objects and the presence of ice was also found by Barucci et al. (2006): all the larger bodies present signatures of ices on their surfaces, while limited or no detections emerged for the smaller objects. This has been interpreted as a natural consequence of different gravity fields, as the large majority of TNOs are too small to retain many volatile species.

Barucci et al. (2008a) identified four different spectral types among TNOs:

- *Methane-dominated:* the very largest TNOs belong to this group, e.g. Pluto, Eris, and Sedna (2003 EL_{61} is the largest TNO that does not show CH_4 signatures). Some objects present both CH_4 and N_2, with methane often dissolved in molecular nitrogen (e.g., Pluto and Sedna). In other objects the CH_4 ice is instead pure (as in the case of 2005 FY_9).

- *Water-ice-dominated:* a second group of TNOs presents spectra with strong H_2O absorptions (Fig. 1.15). The strongest signatures of water ice have been found in objects belonging to the dynamical family of (136108) Haumea. A giant impact on this body is supposed to have generated its dynamical family, as well as its multiple satellite system and its rapid rotation (Brown et al. 2007). Noteworthy, several "water-ice-dominated" TNOs show the 1.65 μm absorption due to crystalline water ice, which implies that during their lifes they have been heated to temperatures above 100/110 K. Since crystalline water ice should be unstable against energetic particle irradiation on timescales of $\sim 10^7$ years, cryovolcanic outgassing has been suggested to explain its detection (Jewitt & Luu 2004).

- *Water-ice spectra with methanol features:* some objects (2002 VE_{95}, 1998 GQ_{21}, and the Centaur Pholus) present a band at 2.27 μm, which is diagnostic of CH_3OH. This suggests a primitive nature of these bodies, since methanol, as other light hydrocarbons, is easily removed by heating in favor of macromolecular carbon.

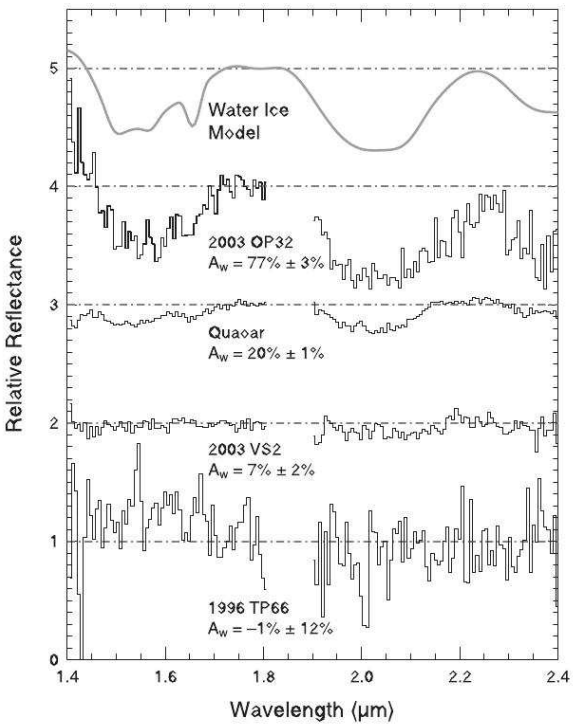

Figure 1.15 – Infrared reflectance spectra of four TNOs. A model spectrum of pure water ice (smooth, gray line) created using a Hapke model and an ice temperature of 40 K with a grain size of 50 μm, is presented for comparison. Quaoar and 2003 OP_{32} show the water ice absorptions at 1.5, 1.65, and 2.0 μm. The quantity Aw, quantifying the amount of water ice absorption at 2.0 μm, is reported next to each spectrum. From Barucci et al. (2008a).

- *Featureless spectra:* many TNOs have featureless spectra, independently of their taxonomic classification (BB to RR). They could have organic-rich surface mantles that cover interior ice.

1.4.3 Rotational properties and densities

The current spin properties of TNOs are supposed to have been strongly affected by the mutual collisions experienced by these bodies. The majority of larger TNOs should rotate with quite primordial angular momentums, while most of the smaller ones are probably fragments generated by disruptive collisions (Davis & Farinella 1997). Sheppard et al. (2008) suggested that an intermediate population of radii $50 \lesssim R \lesssim 100$ km should have been grav-

itationally stable to catastrophic break-up, but with spin properties highly altered over the age of the Solar System.

The largest TNOs have also probably relaxed to equilibrium shapes as a consequence of high internal pressures (Rabinowitz et al. 2006). Assuming a TNO as a cohesionless and strengthless body, i.e. a body with no tensile nor pressure-dependent strength (i.e. a fluid body), its density can be constrained by rotational stability considerations. Hence the analysis of its light curve allows to obtain hints about its internal structure. Indeed, a lower limit to the density of each observed object, below which centrifugal break-up would occur, can be derived by means of the equation:

$$\rho_{min} = \left(\frac{3.3}{P}\right)^2 (1 + \Delta m) \tag{1.11}$$

where P is the rotational period (expressed in hours), Δm is the maximum light curve amplitude, and the resulting density is expressed in g cm^{-3}. This formula is obtained by equating the centrifugal acceleration at the equator of a rotating prolate spheroid with its acceleration of gravity at the surface Pravec & Harris (2000).

Furthermore, possible density ranges can be estimated using the Chandrasekhar (1987) table for rotationally stable Jacobi ellipsoids. Minimum and maximum values of the density are obtained by inputting into the above-mentioned table the computed a/b lower limit (from Eq. 1.10) and $a/b = 2.31$ (more elongated ellipsoids are unstable to rotational fission, Jeans 1919), respectively.

It has been shown that while cohesion does not play a role in determining the permissible spin (for objects of diameter larger than about 10 km), any granular material (e.g., dry sand) can withstand considerable shear stress depending on the confining pressure, as a consequence of the interlocking of the granular particles (Holsapple 2001, 2004, 2007). This shear stress can be parameterized by the so-called angle of friction (ϕ). Typical values of the angle of friction in solid bodies are around 30°, while the fluid assumption implies that $\phi = 0$. Ice acts as a viscous fluid over timescales of years, so an icy body would relax to a fluid shape as described by Chandrasekhar (1987). Hence TNO density estimations through the above procedures are reasonable given the current knowledge and understanding of the physical nature of these bodies. Nonetheless, it should be emphasized that Holsapple showed how a "granular model", with non-zero ϕ, could describe such a body without constraining its shape to be a Maclaurin or Jacobi ellipsoid. This should be taken into account, especially in cases where extremely low (e.g., $\rho \leq 0.5$ g cm^{-3}) or extremely high (e.g., $\rho \geq 2.5$ g cm^{-3}) densities are derived

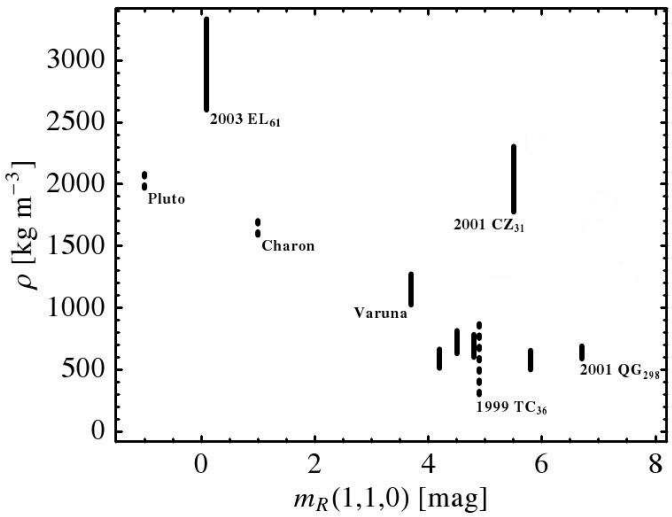

Figure 1.16 – Estimated density ranges of TNOs as a function of their absolute magnitude, before this work. Dashed lines correspond to densities of binary TNOs, estimated based on the satellite orbital properties. Solid lines indicate density ranges estimated from light curves. Figure adapted from Sheppard et al. (2008).

within a strenghtless scenario.

Using available data before this thesis, Sheppard et al. (2008) proposed the existence of a dimension/density trend, with larger (brighter) TNOs being denser than smaller (fainter) ones, suggesting that it could be caused by different porosity and/or rock/ice mass fraction for bodies of different sizes (Fig. 1.16).